JACS
JOURNAL OF THE AMERICAN CHEMICAL SOCIETY
pubs.acs.org/JACS
Article

Elucidation of Factors That Govern the $2e^-/2H^+$ vs $4e^-/4H^+$ Selectivity of Water Oxidation by a Cobalt Corrole

Biswajit Mondal,[‡] Samir Chattopadhyay,[‡] Subal Dey, Atif Mahammed, Kaustuv Mittra, Atanu Rana, Zeev Gross,* and Abhishek Dey*

Cite This: https://dx.doi.org/10.1021/jacs.0c08654

ABSTRACT: Considering the importance of water splitting as the best solution for clean and renewable energy, the worldwide efforts for development of increasingly active molecular water oxidation catalysts must be accompanied by studies that focus on elucidating the mode of actions and catalytic pathways. One crucial challenge remains the elucidation of the factors that determine the selectivity of water oxidation by the desired $4e^-/4H^+$ pathway that leads to O_2 rather than by $2e^-/2H^+$ to H_2O_2. We now show that water oxidation with the cobalt−corrole $CoBr_8$ as electrocatalyst affords H_2O_2 as the main product in homogeneous solutions, while heterogeneous water oxidation by the same catalyst leads exclusively to oxygen. Experimental and computation-based investigations of the species formed during the process uncover the formation of a Co(III)−superoxide intermediate and its preceding high-valent Co−oxyl complex. The competition between the base-catalyzed hydrolysis of Co(III)−hydroperoxide $[Co(III)-OOH]^-$ to release H_2O_2 and the electrochemical oxidation of the same to release O_2 via $[Co(III)-O_2^{\bullet}]^-$ is identified as the key step determining the selectivity of water oxidation.

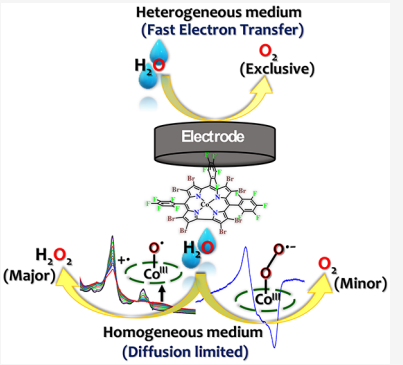

INTRODUCTION

A desirable goal of water oxidation, which has now been identified as the bottleneck of the water-splitting reaction, is to obtain selectivity over H_2O_2, via $2e^-/2H^+$ oxidation, or O_2, via a $4e^-/4H^+$ oxidation.[1−19] Product selectivity is one of the key aspects in multiproton/multielectron transformation, and it is a contemporary interest in the electrochemical oxygen reduction reaction. Similarly, water can be oxidized via $2e^-/2H^+$ to form H_2O_2 (E^0 = 1.76 V vs NHE) or by $4e^-/4H^+$ to afford O_2 (E^0 = 1.23 V vs NHE). Of course, water oxidation to oxygen is thermodynamically more favorable than its oxidation to H_2O_2, and hence, the issue has not attracted attention until recently when H_2O_2 was reported as a product during water oxidation.[20−22] H_2O_2 is an inorganic bulk material, and logically, its electrosynthesis from water is also a topic of interest. The erstwhile focus of the water oxidation community has been accelerating the rate and efficiency of the water oxidation process using cheap first-row transition-metal-based materials and complexes.[23−30] Several Co-based complexes/composites have been recently used as catalysts for water splitting in this regard.[31−49] Macrocyclic corrole, a porphyrin-like moiety, has recently emerged as a unique ligand to carry out several catalytic transformations. It has the capability to support both high and low formal metal oxidation states.[50−57] This nature of the corrole ligand encouraged exploration of its potential for electrocatalysts for supporting the oxygen evolution reaction (OER), hydrogen evolution reaction (HER), oxygen reduction reaction (ORR), etc.[23,58−67]

Recently, a system for molecular OER was reported containing a hangman β-octafluoro corrole cobalt complex with a high-valent Co(IV) corrole cation radical as the precatalyst.[68] β-Halogen substitution on the corrole ring in a metallocorrole complex has a dominant effect in controlling the redox potential of the metal and their subsequent reactivity.[61,69] Furthermore, the β-positions of the corrole macrocycle are prone to oxidation, leading to dearomatization.[70] Hence, β-halogenation helps in rendering stability to the system.[50,55] Nevertheless, this catalyst is efficient for water oxidation in aqueous medium over a large range of pH values with considerably high turnovers.[68] There are theoretical reports on the mechanism of cobalt corrole-based water oxidation catalysis.[71,72] However, identification of the reactive intermediates involved is the key for understanding the mechanism of action which precedes rational design of better catalysts.

With the development of a number of reasonable catalysts, the focus has now shifted toward understanding the factors that control the selectivity of the process. To be able to tune selectivity one needs a detailed understanding of the mechanism of water oxidation. There has been some

Received: August 12, 2020

https://dx.doi.org/10.1021/jacs.0c08654
J. Am. Chem. Soc. XXXX, XXX, XXX−XXX

development in understanding the mechanism of Co−Pi and Ru catalysts.[73−75] A Co−Pi catalyst, which is well known for its high catalytic activity in neutral water and a Co(IV)−OH/Co(III)−O$^{\bullet}$ intermediate, is proposed to be involved in the catalytic process.[76−79] Very recently, Hu et al. studied the mechanism of the OER with cobalt oxyhydroxide, and the in situ Raman data reveal the involvement of a superoxide species at the same time as the oxidation of CoOOH to CoO_2, which occurs before the onset of the OER.[80] Through a labeling experiment it is concluded that this superoxide species is a precursor to dioxygen. It is also proposed that O−O bond formation took place prior to the rate-determining step, which contradicts most of the mechanisms reported in the literature.[81−84] Rational design of efficient catalysts using mechanistic insights obtained from spectrochemical data has been recently demonstrated by achieving a facile and selective $4e^-/4H^+$ ORR in simple mononuclear iron porphyrins by identifying the chemical steps responsible for product selectivity.[85−88] Similar mechanism-based catalyst design is being undertaken for water oxidation as well.[10,89] In particular, the ability to control the chemical steps involved in water oxidation that determine the product selectivity can enable selective production of O_2 and H_2O_2 using the catalyst.

Here, we report that the tris(5,10,15-pentafluorophenyl)-2,3,7,8,12,13,17,18-octabromocobalt corrole ($CoBr_8$; Figure 1)

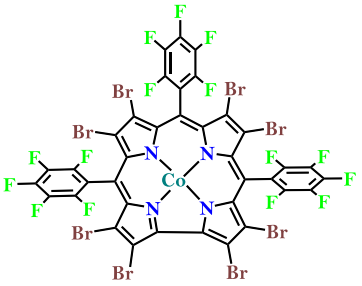

Figure 1. Chemical structure of the investigated cobalt(III) corrole complex ($CoBr_8$).

complex shows water oxidation activity under homogeneous and heterogeneous electrochemical conditions. Oxidation of H_2O leads to H_2O_2 under homogeneous electrochemical conditions and O_2 under heterogeneous conditions. A Co(III)−corrole cation radical intermediate is trapped and identified during homogeneous water oxidation. A Co(III)−superoxide, $[Co(III)-O_2^{\bullet}]^-$ intermediate is also identified during homogeneous electrocatalysis, providing direct evidence for the O−O bond formation process. A competition between the base-catalyzed hydrolysis of intermediate species to release H_2O_2 or the electrochemical oxidation of $[Co(III)-O_2^{\bullet}]^-$ to release O_2 is identified as the key step in determining the selectivity of $2e^-$ vs $4e^-$ H_2O oxidation.

RESULTS

Homogeneous Electrochemistry in an Acetonitrile/Water Mixture. Cyclic voltammetry (CV) of the complex in degassed acetonitrile shows two quasireversible waves at 0.95 and 1.4 V (Figure 2, red). These processes are best described as [corrole−Co(III)−OH_2]/ [corrole$^{\bullet+}$−Co(III)−OH] at 0.95 V and [corrole$^{\bullet+}$−Co(III)−OH]/ [corrole$^{\bullet+}$−Co(III)−O$^{\bullet-}$] at 1.4 V.[71,90] Upon addition of aqueous base, a catalytic current is observed with an onset corresponding to the redox

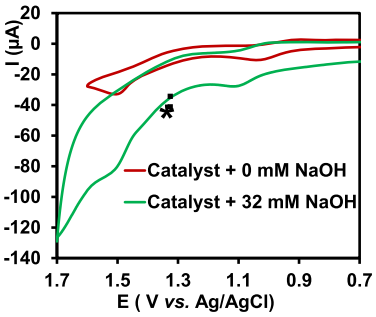

Figure 2. Homogeneous electrocatalytic water oxidation with $CoBr_8$. Cyclic voltammograms of 0.5 mM $CoBr_8$ in degassed acetonitrile in the absence (red) and presence of 32 mM NaOH (green) using GCE as the working electrode, Pt as the counter electrode, and Ag/AgCl as the reference electrode. Scan rate = 100 mV/s. Potential at which electrochemical experiments were performed is indicated with an asterisk.

wave at 1.4 V, and the current increases with increasing amount of base, suggesting the catalytic process to be associated with the oxidation of this aqueous hydroxide species. The catalytic onset potential also shifts to a lower value with increasing concentration of base, spanning from 1 mM to 32 mM (Figure S1), suggesting that the oxidation is coupled to a deprotonation step as may be expected for a proton-coupled electron transfer (PCET) process. Furthermore, the catalysis is first order with respect to the catalyst concentration, suggesting it to be a single-site molecular catalyst (Figure S2), and simultaneously eliminates the possibility of formation of any Co−oxide films on the electrode surface as observed by many Co-based WOC systems (see Supporting Information for further details).[91,92] The linear increase of the square of the water oxidation current (i_p) with base concentration indicates that the catalytic process is first order with respect to base (Figure S3). The decrease in catalytic current with increasing scan rate indicates a mass transfer chemical step, presumably an O−O bond formation step (Figure S4), as the rate-determining step of the reaction. The evolved O_2 was detected in situ by reverse cathodic scan (Figure S5). A controlled potential electrolysis (CPE) experiment was performed at 1.3 V with 0.5 mM catalyst in acetonitrile having 32 mM aqueous NaOH (Figure S6). The Faradaic yield (FY) thus calculated for water oxidation to oxygen is determined to be 18% by measuring the volume of oxygen produced (0.2 mL) by displacement of water at 1 atm pressure (Figure S6). Water oxidation can lead to formation of O_2 as well as H_2O_2. Simultaneously, H_2O_2 is detected in solution using a xylenol orange assay (detailed description is given in the Supporting Information, Figure S7). The FY of H_2O_2 production is 70 ± 2%. Thus, in acetonitrile:water medium, both the $2e^-$ and the $4e^-$ oxidation products H_2O_2 and O_2, respectively, are observed. The yield of H_2O_2 is higher than the yield of O_2 under these experimental conditions, and the total amount of H_2O_2 and O_2 detected yields 88% FY for the overall process.

Heterogeneous Electrochemistry. To gain further insight into the process, the $CoBr_8$ complex is physiadsorbed on edge-plane graphite (EPG) electrode, and this electrode shows water oxidation in aqueous buffered solutions, spanning pH values from 7 to 12. The electrocatalytic water oxidation current (absent in a bare EPG electrode; Figure S8) increases with increasing pH (analogous to increasing base concen-

https://dx.doi.org/10.1021/jacs.0c08654
J. Am. Chem. Soc. XXXX, XXX, XXX−XXX

tration in acetonitrile solution), and simultaneously the onset potential of catalysis shifts to lower values (Figure 3A). At pH

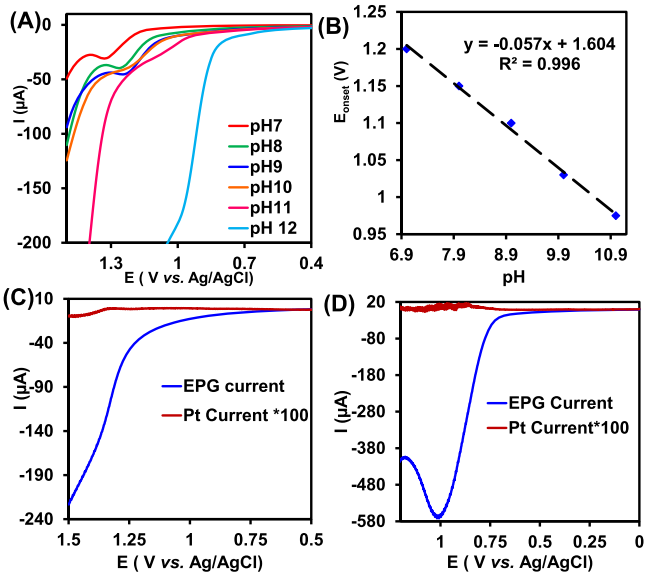

Figure 3. Heterogeneous electrocatalytic water oxidation with $CoBr_8$. (A) LSV of $CoBr_8$ physiadsorbed on EPG electrode at different pHs, (B) plot of peak potential vs pH for $CoBr_8$, and H_2O_2 detection under heterogeneous conditions using RRDE with the Pt ring encircling the EPG electrode kept at a constant potential of (C) 0.4 V at pH 10 and (D) 0.2 V at pH 12. Rotation speed = 300 rpm for RRDE. Scan rate of 50 mV/s for LSV and 10 mV/s for RRDE using Pt as the counter electrode and Ag/AgCl (saturated KCl) as the reference electrode.

12 the catalytic onset potential ($E^0_{onset,}$ potential at which the catalytic current is ~10 times with respect to the background current at same pH) for $CoBr_8$ is 0.84 V. A plot of the onset potential (E_{onset}) versus pH shows a monotonic decrease from pH = 7 to 11 with a slope of 57 mV/pH for $CoBr_8$ (Figure 3B), suggesting the involvement of a $1H^+/1e^-$ PCET step (i.e., ΔE = 59 mV/pH decade) as the potential-determining step (pds) of the water oxidation process in an aqueous environment, and this reinforces the involvement of PCET in homogeneous nonaqueous medium. At further higher pH (pH = 12) a sharp jump of the catalytic onset potential is seen and is presumably associated with a pK_a event of $[Co(III)-OOH]^-/[Co(III)-O_2]^{2-}$ and not likely due to formation of cobalt−oxide or other degradation as this process is reversible with the change of pH. Bubble formation on the electrode surface occurs during the anodic run consistent with oxygen gas evolution due to water oxidation (Figure S9). In a rotating ring disk electrochemistry (RRDE) setup, any H_2O_2 formed can be detected by a Pt ring that encircles the working electrode, which is held at a constant potential where it oxidizes the H_2O_2, produced at the working electrode and diffused outward toward it due to the hydrodynamic flow created by the rotation of the shaft bearing the electrode, to O_2. No H_2O_2 is detected in this setup, indicating that H_2O is exclusively getting oxidized by $4e^-$ to O_2 under heterogeneous electrochemical conditions in water (Figure 3C and 3D). This is different from the observation in organic medium where 70% H_2O_2 formation was detected. It is worth noting from the thermodynamic analysis performed under the electrolysis conditions in homogeneous water oxidation that the applied potential is enough to drive water oxidation to both oxygen and hydrogen peroxide (Figure S10). This holds true for heterogeneous water oxidation as well (Figure S11, see the Supporting Information for details). The fact that water oxidation to hydrogen peroxide ($E^0_{H2O/H2O2(aq)}$ = 1.76 V) is always thermodynamically more uphill than water oxidation to oxygen ($E^0_{O2/H2O(aq)}$ = 1.23 V) and in spite of having enough driving force in both homogeneous and heterogeneous conditions for both processes, in homogeneous conditions hydrogen peroxide is the major product and in heterogeneous conditions exclusively oxygen is formed due to water oxidation. These results suggest that there is a more relevant kinetic pathway that dictates the product selectivity for water oxidation with this catalyst (vide infra).

UV−vis Spectroelectrochemistry. This difference in product selectivity in water oxidation is very interesting, and this caused us to further study the mechanism of the water oxidation process. In the literature, Nocera et al.[68] and Shaik et al.[72] proposed a formal Co(V) or Co(IV) cation radical to be the active form of the cobalt corrole-based water oxidation catalyst. However, recently, Cramer et al.[71] and Cao et al.[59] proposed a $[corrole^{\bullet+}-Co(III)-O^{\bullet-}]$ species to be active form for such catalysis. In our pursuit, the mechanistic details of the water oxidation by $CoBr_8$ are investigated using spectroelectrochemical techniques.

The initial Co(III) corrole has a well-defined Soret band at 448 nm and a less intense Q-band at 608 nm in acetonitrile, and the intensity of the bands decreases upon electrochemical oxidation in acetonitrile of the species at 1.3 V, indicating consumption of the initial species (Figure 4A). In the presence of aqueous base, when the electrolysis is performed at 1.3 V, the Soret band at 448 nm decreases in intensity and red shifts to 454 nm and the band at 608 nm loses its intensity (Figure 4B). Thus, during electrolysis in the presence of base (i.e.,

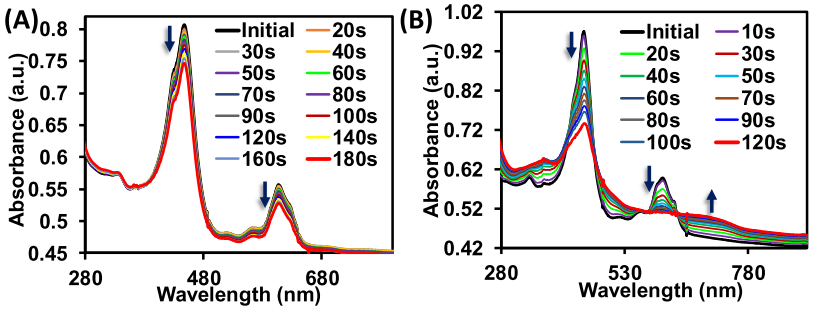

Figure 4. UV−vis spectroelectrochemistry in noncatalytic and catalytic conditions. UV−vis spectral changes of $CoBr_8$ during (A) controlled potential oxidation at 1.3 V in acetonitrile with water, containing 100 mM TBAP, and (B) the same with aqueous base.

https://dx.doi.org/10.1021/jacs.0c08654
J. Am. Chem. Soc. XXXX, XXX, XXX−XXX

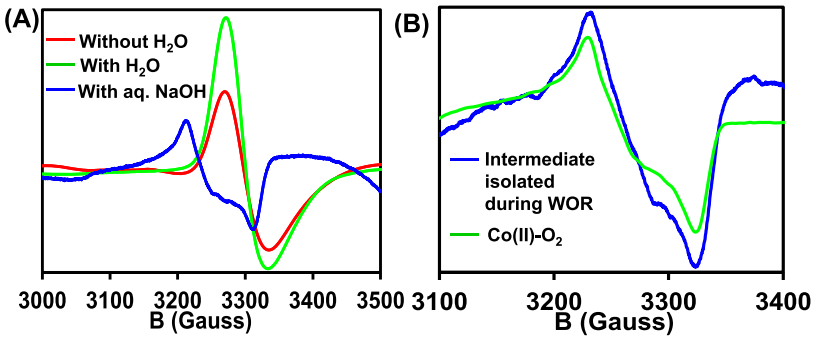

Figure 5. EPR of cobalt(III)−superoxide intermediate involved in water oxidation. EPR spectra of (A) the oxidized $CoBr_8$ produced by electrochemical oxidation in degassed acetonitrile (red), in water:acetonitrile mixture (green), in aqueous-base:acetonitrile mixed solvent (blue), and (B) Co(III) superoxo corrole as obtained by oxygenation of the reduced Co(II) corrole (green) and after electrochemical oxidation in degassed aqueous-base:acetonitrile solvent mixture (blue).

when the catalyst is involved in a steady state OER), multiple well-defined isosbestic points in the spectra serve to indicate formation of a single oxidation product. The new broad band that starts growing at 722 nm suggests formation of a high-valent Co−O species as the electrolysis proceeds.[51,93] Density functional theory (DFT) calculations on a Co(III)−oxyl corrole cation radical species predict a broad absorption band centered around 700 nm, consistent with the experimental data (Figure S12).

Electron Paramagnetic Resonance. The species accumulated during water oxidation is further investigated using EPR. When 0.5 mM catalyst solution in acetonitrile is oxidized with ceric ammonium nitrate (CAN) solution in MeOH, a radical signal (g = 1.98) is observed (Figure S13). The observed g value is characteristic of the organic radical, and based on the previous literature on high-valent corroles, this species is likely to be a Co(III) corrole radical cation rather than Co(IV) corrole.[94] When a 0.5 mM catalyst solution in acetonitrile is subjected to controlled potential electrolysis (CPE) at 1.3 V with or without water, the same radical species, Co(III) corrole radical cation, with g value = 1.98 is formed (Figure 5A, green and red). Thus, the redox event at 1.3 V can be assigned as a Co−corrole/Co−corrole π-cation radical. DFT calculations on a hypothetical one-electron-oxidized Co(III) corrole show that in the calculated spin densities of the complexes with neutral axial ligand (py, H_2O) ∼100% of the spin resides on the corrole ring (Figure S14, Table ST1). This suggests the one-electron-oxidized form of Co(III) corrole is a Co(III) corrole cation radical rather than Co(IV) corrole, consistent with the previous theoretical calculations.[71] This observation is also supported by the EPR data obtained during chemical oxidation of the sample with CAN and electrochemical oxidation of the sample in acetonitrile with or without water (Figure S13, Figure 5A, red and green).

Electrolysis at the same potential in the presence of aqueous base renders a new rhombic EPR signal with the g value shifted to >2 (g value = 2.01) (Figure 5B, blue) and the signal is significantly different from a Co(II) corrole, which shows a very anisotropic g value.[95] Furthermore, the signal of the species immediately after water oxidation is identical with the spectrum that is obtained from oxygenation of a Co(II) corrole at cryogenic temperatures (Figure 5B, green). Previous reports[58,94] show that oxygenation of Co(II) corrole results in formation of a $[Co(III)-O_2^{\bullet}]^-$ metastable species which is EPR active with g values close to 2.[95] Thus, part of the reactive species that is obtained via sampling of the bulk during controlled potential catalytic turnover of H_2O to O_2 is identified as $[Co(III)-O_2^{\bullet}]^-$. Integration of the signal (EPR spin quantification) represents 15 ± 5% of the species in solution. The EPR signal decays (total spin loss ≈ 70−74%) within minutes (i.e., a half-life, $t_{1/2}$ of 60 s) on standing (Figure S15), indicating that it is not a stable product of O_2 binding to a Co^{II} species. The 15% population of $[Co(III)-O_2^{\bullet}]^-$ is very close to 18% FY as observed for formation of O_2, clearly indicating that $[Co(III)-O_2^{\bullet}]^-$ is the predecessor to the O_2 evolved.

DISCUSSION

The OER data of brominated cobalt corrole show that during homogeneous conditions the amount of H_2O_2 produced is 70% and only 18% O_2 is generated. However, under heterogeneous conditions, in an aqueous medium, the complex produces O_2 exclusively. Heterogeneous electrocatalysis distinguishes itself from homogeneous electrocatalysis, resulting in much faster electron transfer (ET) rates from the electrode to the catalyst, directly absorbed on the electrode. In homogeneous electrocatalysis the ET rate is limited by catalyst diffusion to the electrode. Thus, the observed difference in selectivity in the OER between heterogeneous and homogeneous conditions likely originates from a key ET step in the mechanism. Spectroelectrochemistry data indicate that while in the absence of base (substrate) the oxidation results in formation of a Co(III)corrole radical species, during catalysis (in the presence of base) a $[Co(III)-O_2^{\bullet}]^-$ species is observed. A plausible mechanism has been proposed for the process (Scheme 2). Spectroelectrochemical data suggest species **1** gets oxidized to **2** (first redox event). Species **2** is characterized through EPR during electrocatalytic water oxidation in the presence of H_2O and is likely to be a Co(III) corrole cation radical, consistent with a previous literature report.[59] The second oxidation process is responsible for water oxidation, and based on the theoretical data in the literature, $[Cor^{\bullet+}-Co^{III}-O^{\bullet-}]$ (**3**) is proposed to be the active species for water oxidation. Nocera et al. also proposed a formal Co(V) species as the active water oxidation species.[68] This species is formed through a PCET process from **2**, which is consistent with the 57 mV/pH shift in the onset potential under heterogeneous conditions and is the potential-determining step (pds). Species **3** then undergoes a hydroxide nucleophilic attack which is likely to be the rds from the electrochemical data analyzed at the mass transfer region where electron transfer rates are fast. Nucleophilic attack of

https://dx.doi.org/10.1021/jacs.0c08654
J. Am. Chem. Soc. XXXX, XXX, XXX−XXX

Scheme 1. Plausible Mechanism of Water Oxidation by Co Corrole[a]

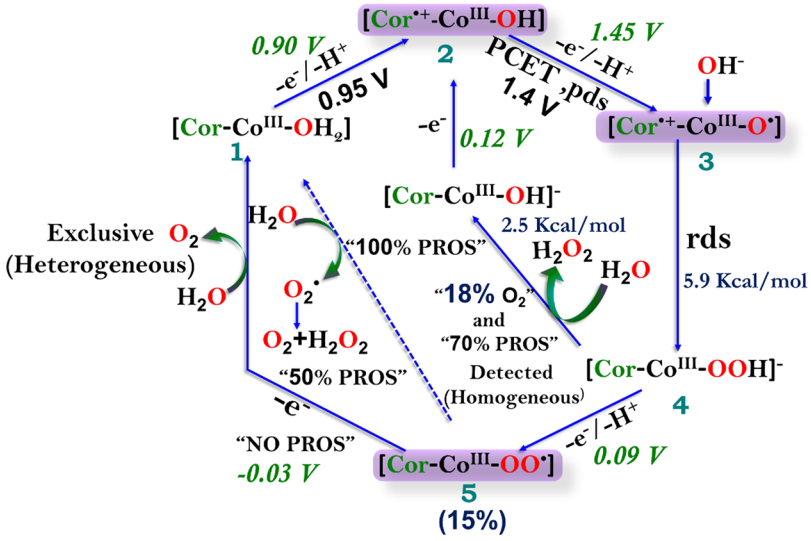

[a]Species in violet rectangles are identified: **2** by chemical and spectroelectrochemical 1-electron oxidation, **3** by spectroelectrochemical 2-electron oxidation, **5** by EPR of an interrupted controlled-potential water oxidation solution. DFT-calculated potentials are given in green, whereas experimental values are given in black; these are all reported vs AgCl/Ag. Change in free energies for the chemical steps are given in navy blue.

H_2O or OH^- on **3** yields a $[Co(III)-OOH]^-$ species (**4**). Under homogeneous conditions, $[Co(III)-OOH]^-$ undergoes competitive hydrolysis to afford the $2e^-$ oxidation product H_2O_2. The $[Co(III)-OOH]^-$ species is oxidized in a PCET step, resulting in a $[Co(III)-O_2^{\bullet}]^-$ species which is identified through EPR. Oxidation of the $[Co(III)-O_2^{\bullet}]^-$ species at the electrode yields the $4e^-$ oxidation product O_2. Note that an Mn−corrole−peroxide intermediate has also been identified in mass spectrometry during chemical oxidation of Mn corrole with *t*BuOOH.[96]

Our kinetic data in homogeneous medium further reveal that the reaction is first order in both catalyst and base concentration and that the catalytic current decreases with increasing scan rate, suggesting a mass transfer step as the rate-limiting step of the overall reaction. This step is likely to be the nucleophilic hydroxide attack on the $[Cor^{\bullet+}-Co^{III}-O^{\bullet-}]$ species. This is reasonable since the latter species built up in a significant amount during spectroelectrochemistry in the presence of base during catalytic turnovers (Figures 4B and S16). The band at ∼700 nm is attributed to the high-valent cobalt oxyl species as confirmed by the time-dependent density functional theory calculations (Figure S12). Nevertheless, the hydroxide attack on $[Cor^{\bullet+}-Co^{III}-O^{\bullet-}]$ affords a hydroperoxide intermediate which is expected to be readily deprotonated to a peroxide intermediate under alkaline conditions followed by one-electron oxidation at high anodic potential to afford $[Co(III)-O_2^{\bullet}]^-$. This mechanism of cobalt−superoxide formation during water oxidation is different from the recently reported mechanism of Hu et al., where the hydroperoxide deprotonation and oxidation pathway is ruled out and instead a combination of two lattice O atoms as the cobalt−superoxide formation step is invoked.[80] However, the pathway discussed in this report bears similarity to the mechanism proposed by Frei et al., where water nucleophilic attack followed by oxidation leads to the cobalt−superoxide intermediate in a near neutral photocatalytic OER. A Mn corrole is also reported in this regard to afford an Mn−OOH intermediate during the OER.[97] It is further interesting in this report that these intermediates intercept the product selectivity in the water oxidation reaction. The fact that under homogeneous electrocatalytic conditions 18% O_2 is formed and 70% is H_2O_2 suggests that there occurs a competition among hydrolysis of hydroperoxide and superoxide intermediates to afford H_2O_2 and oxidation of the cobalt−superoxide intermediate (∼15% as detected in spectroelectrochemistry) to release oxygen. Thus, this observation is in congruence with Hu et al. that a cobalt−superoxide species is precursor to oxygen formation but with a contrast that this selectivity-determining step occurs after the rate-determining step of the reaction (if cobalt−superoxide oxidation would be rate limiting in this case, the amount of H_2O_2 would be 50% at maximum; vide infra). The occurrence of a selectivity-determining step after the rate-limiting step is very common in the ORR.[98] These steps become relevant in homogeneous water oxidation where the electron transfer is limited by diffusion and these intermediates can undergo hydrolysis to afford H_2O_2. However, in heterogeneous conditions, where the electron transfer steps are fast, these intermediates after the rate-limiting step become less prominent, prone to hydrolysis, and afford oxygen as the exclusive product. The fact that even under nonaqueous medium when the catalyst is adsorbed on a graphite electrode with Nafion only 6.1% H_2O_2 is detected in the ring current in the rotating ring disk electrochemistry (RRDE) experiment indicates that rapid ET leads to selectivity for O_2 formation over H_2O_2 (Figure S21A and S21B).

DFT calculations of the proposed mechanism show reasonably good agreement between the calculated potential and the experimentally observed potential for the first two oxidation steps (**1**→ **2** and **2**→ **3**, Scheme 1: experimental data in black and theoretically calculated data in green). Formation of the O−O bond via a nucleophilic attack of hydroxide on the oxyl species **3** involves a thermodynamic barrier and is consistent with the observation of the same species in solution in operando (Figures 4B and S12). Hydrolysis of the $Co^{III}-OOH$ species (**4**) is calculated to have a small endergonic requirement, suggesting that the release of H_2O_2 from this species is likely consistent with 70% H_2O_2 observed during homogeneous water oxidation. The calculated potentials for

https://dx.doi.org/10.1021/jacs.0c08654
J. Am. Chem. Soc. XXXX, XXX, XXX−XXX

Scheme 2. Probable Fate of $[Cor-Co^{III}-OOH]^-$ and $[Cor-Co^{III}-OO^{\bullet}]^-$ [a]

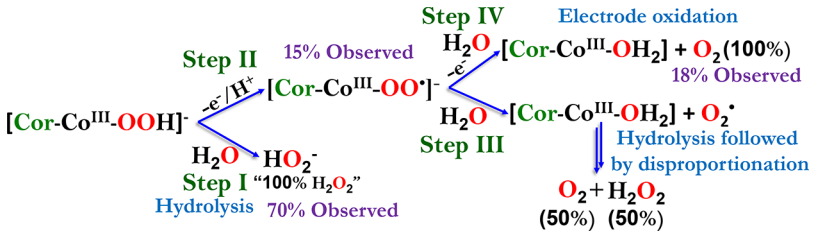

[a]The percent of H_2O_2 that should be detected is indicated in parentheses.

the oxidation of **4** and **5** (0.09 and −0.03 V, respectively) which lead to release of O_2 are thermodynamically downhill relative to the calculated PCET oxidations of **2** to **3** (0.9 and 1.45 V, respectively). Thus, unsurprisingly, the applied potential required to achieve oxidation of **2** to **3** is sufficient to drive the oxidation of both **4** and **5**.

The 70% H_2O_2 and 18% O_2 observed under homogeneous conditions also help diagnose the steps in the mechanistic cycle. Hydrolysis of the proposed $[Co(III)-OOH]^-$ intermediate would lead to as much as 100% H_2O_2 (step I, Scheme 2). On the other hand, this species can undergo deprotonation along with $1e^-$ oxidation to the $[Co(III)-O_2^{\bullet}]^-$ species (step II, Scheme 2). Involvement of a $[Co(III)-O_2^{\bullet}]^-$ in water oxidation, identified in this investigation, has recently been proposed for a Co-based material as a kinetically competent intermediate.[97] The $[Co(III)-O_2^{\bullet}]^-$ species can hydrolyze to generate Co(III) and $O_2^{\bullet-}$ (step III, Scheme 2). In the case of hydrolysis of the $[Co(III)-O_2^{\bullet}]^-$ species, the resultant $O_2^{\bullet-}$ would disproportionate to yield 50% O_2 and 50% H_2O_2, i.e., a maximum 50% FY for H_2O_2. Since, we only observe 15% of $[Co(III)-O_2^{\bullet}]^-$, which accounts for the oxygen formed, it is unlikely that this species hydrolyzes. This is not consistent with the 70% H_2O_2 under homogeneous conditions. Alternatively, oxidation of the same $[Co(III)-O_2^{\bullet}]^-$ species at the electrode will generate Co(III) + O_2 (step IV, Scheme 2) with no H_2O_2 formation. Thus, 70% H_2O_2 observed under homogeneous conditions suggests competition between the hydrolysis of a $[Co(III)-OOH]^-$ intermediate and the PCET oxidation of this species to $[Co(III)-O_2^{\bullet}]^-$. Oxidation of the $[Co(III)-OOH]^-$ can be expected to be much faster under heterogeneous conditions where the catalyst is directly attached to the electrode. Thus, under heterogeneous conditions, oxidation of the $[Co(III)-OOH]^-$ is faster than its hydrolysis, which drives selective $4e^-$ oxidation of water to O_2. Under homogeneous conditions hydrolysis of the $[Co(III)-OOH]^-$ species is faster than its diffusion-controlled oxidation at the working electrode, resulting in 70% H_2O_2. The rest of the species (30%) is converted to $[Co(III)-O_2^{\bullet}]^-$ through electrode oxidation (step II, Scheme 2), which is observed, and the amount of this species detected is ∼15% (EPR spin quantification). This $[Co(III)-O_2^{\bullet}]^-$ species thus generated and observed (∼15%) is oxidized to afford the ∼18% O_2 collected during homogeneous water oxidation.

CONCLUSION

In summary, cobalt corrole can be used as an efficient water splitting catalyst facilitating both proton reduction to H_2 and water oxidation to O_2 under both homogeneous and heterogeneous conditions in organic and aqueous medium, respectively.[60,68] Here, it is demonstrated that the selectivity of the OER can be tuned by changing the reaction conditions. Homogeneous water oxidation with $CoBr_8$ affords H_2O_2 as the main product, while heterogeneous water oxidation leads to O_2 exclusively. In situ spectroelectrochemical investigation of the $CoBr_8$ involved in homogeneous electrocatalytic water oxidation shows formation of a $[corrole^{\bullet+}-Co(III)-O^{\bullet}]$ and a $[Co(III)-O_2^{\bullet}]^-$ intermediate, providing direct evidence for the mechanism of O−O bond formation from water. Competition between the base-catalyzed hydrolysis of a $[Co(III)-OOH]^-$ intermediate species to release H_2O_2 and its the electrochemical oxidation to $[Co(III)-O_2^{\bullet}]^-$ is identified as the key step determining the selectivity for $2e^-$ vs $4e^-$ H_2O oxidation. Under homogeneous conditions where its oxidation is slower than its hydrolysis, 70% H_2O_2 is produced. Alternatively, under heterogeneous conditions where its direct attachment to the electrode results in rapid ET, O_2 is observed as the sole product of the OER. These results herald a new catalyst design and reaction engineering approach to control the rates and selectivity of water oxidation by cobalt-based molecular complexes. The fact that the same intermediates were observed in Co-based materials further reinstates the generality of these findings in water oxidation catalysis.

EXPERIMENTAL METHODS

Materials and Instrumentation. All chemicals were commercially available, of the highest purity grade, and used without further purification. Tetrabutylammonium perchlorate (TBAP), potassium hexafluorophosphate (KPF_6), ceric ammonium nitrate (CAN), and sodium hydroxide pellet as base in aqueous media were purchased from Sigma-Aldrich. Disodium hydrogen phosphate dihydrate ($Na_2HPO_4{\cdot}2H_2O$), potassium chloride (KCl), potassium nitrate (KNO_3), and the solvents (HPLC grade) used in the electrochemical studies were purchased from Merck. Acetonitrile was dried over calcium hydride and stored over 4 Å molecular sieves before being used in the electrochemical experiments. Glassy carbon (GC) electrodes, edge-plane graphite (EPG) electrodes, platinum counter electrode, and sealed aqueous Ag/AgCl (saturated KCl) electrodes were purchased from Pine Instruments, USA. The spectroelectrochemical UV−vis cell was purchased from ALS, Japan.

All electrochemical experiments were performed using a CH instruments (CHI710d) electrochemical analyzer (bipotentiostat). RRDE data were collected using the RRDE setup from Pine Instruments, USA (E6 series with change disc tips with AFE6M rotor). All electron spin resonance (ESR) spectra were collected at 77 K using a Jeol ESR instrument. UV−vis absorption data were taken in an AgilentTtechnologies spectrophotometer model 8453 fitted with a diode-array detector.

Construction of the Modified Electrode (EPG Electrode). A 100 μL amount of 1 mM catalyst in chloroform was deposited on a freshly cleaned EPG electrode mounted on an RRDE setup. Once the solvent was fully evaporated, the surface was rinsed with chloroform, ethanol, and Milli-Q water gradually and thoroughly dried under N_2 atmosphere before each of the electrochemical experiments.

https://dx.doi.org/10.1021/jacs.0c08654
J. Am. Chem. Soc. XXXX, XXX, XXX−XXX

Electrocatalytic Water Oxidation. In all of the electrochemical experiments, aqueous Ag/AgCl (saturated KCl) and Pt were used as the reference and counter electrodes, respectively, unless otherwise mentioned.

Homogeneous Electrochemistry. A 0.5 mM solution of the complex was prepared in degassed acetonitrile for the electrochemical studies. TBAP was used as the supporting electrolyte. Glassy carbon (GC), sealed aq. Ag/AgCl (saturated KCl), and Pt wire were used as the working, reference, and counter electrodes, respectively. All CVs were collected with scan rates of 100 mV/s. For the electrocatalytic water oxidation studies in acetonitrile:water medium, sodium hydroxide was used as the aqueous base (1 M initial stock; the base equivalents were added as per the millimolar amount depicted) and H_2O_2 was the product detected by xylenol orange assay (sensitivity limit 15 ng/mL). Turbidity occurs beyond 40 mM base concentration. The homogeneity test was performed under the operating conditions (see Supporting Information for details; Figure S19A–D), and no nanoparticle formation was detected. The background current in the absence of catalyst is also provided in the Supporting Information (Figure S20).

Heterogeneous Electrochemistry. The edge-plane pyrolytic graphite electrode (EPG) was cleaned using an electrochemical polishing kit and inserted into the RRDE tip. It was cleaned thoroughly with triple-distilled water, ethanol, and chloroform and dried using N_2. The chloroform solution of the catalyst was loaded on to the EPG electrode and left for 10 min. It was rinsed with chloroform, ethanol, and triple-distilled water and dried with N_2 gas, which was then mounted on the rotor and immersed into a cylindrical glass cell equipped with Ag/AgCl reference and Pt wire counter electrodes. LSV data were collected at a scan rate of 50 mV/s and RRDE data were collected at a scan rate of 10 mV/s, and the rotation speed was maintained at 300 rpm. The experiments were carried out in phosphate buffer with KPF_6 as supporting electrolyte.

Spectroelectrochemical Experiments. *UV–vis Spectroelectrochemistry.* Spectral changes were measured with UV–vis spectroscopy with the catalyst in dry acetonitrile and with the catalyst in acetonitrile:aqueous base (32 mM) during controlled potential electrolysis at 1.3 V.

Electron Paramagnetic Resonance (EPR) Spectroscopy. A 0.5 mM solution of the complex in degassed acetonitrile was electrolyzed under anaerobic conditions at potentials as mentioned in each case for 0.5 h using a GCE working electrode, Ag/AgCl reference electrode, and Pt wire counter electrode. TBAP was used as the supporting electrolyte. Samples for EPR were collected from the electrolytic solution after 0.5 h of electrolysis at 1.3 V and frozen in liquid N_2, and the EPR data were recorded for these samples at 77 K.

Density Functional Theory Calculations. All of the calculations were performed on the Inorganic HPC cluster at IACS using the Gaussian 03 software package.[99] The geometries were optimized with the spin-unrestricted formalism using both the BP86 functional and the 6-311G* basis set for Co and the 6-31G* basis set for other atoms. Frequency calculations were performed on each optimized structure using the same basis set to ensure that it was a minimum on the potential energy surface. Total energy calculations were performed using the 6-311+G* basis set in acetonitrile solvent (PCM) and a convergence criterion of 10^{-8} Hartree.[100,101] Further details on the solvation energies are given in the Supporting Information.

■ ASSOCIATED CONTENT

Supporting Information

The Supporting Information is available free of charge at https://pubs.acs.org/doi/10.1021/jacs.0c08654.

Details of the experimental procedure, materials, additional electrochemical and spectroscopic data, and coordinates of the optimized geometries (PDF)

■ AUTHOR INFORMATION

Corresponding Authors

Abhishek Dey − *School of Chemical Sciences, Indian Association for the Cultivation of Science, Kolkata 700032, India;* orcid.org/0000-0002-9166-3349; Email: icad@iacs.res.in

Zeev Gross − *Schulich Faculty of Chemistry, Technion-Israel Institute of Technology, Haifa 3200008, Israel;* orcid.org/0000-0003-1170-2115; Email: chr10zg@technion.ac.il

Authors

Biswajit Mondal − *School of Chemical Sciences, Indian Association for the Cultivation of Science, Kolkata 700032, India;* orcid.org/0000-0002-2339-3076

Samir Chattopadhyay − *School of Chemical Sciences, Indian Association for the Cultivation of Science, Kolkata 700032, India;* orcid.org/0000-0003-4759-0362

Subal Dey − *School of Chemical Sciences, Indian Association for the Cultivation of Science, Kolkata 700032, India;* orcid.org/0000-0002-5626-4879

Atif Mahammed − *Schulich Faculty of Chemistry, Technion-Israel Institute of Technology, Haifa 3200008, Israel*

Kaustuv Mittra − *School of Chemical Sciences, Indian Association for the Cultivation of Science, Kolkata 700032, India;* orcid.org/0000-0003-2325-1972

Atanu Rana − *School of Chemical Sciences, Indian Association for the Cultivation of Science, Kolkata 700032, India;* orcid.org/0000-0002-2397-5869

Complete contact information is available at: https://pubs.acs.org/10.1021/jacs.0c08654

Author Contributions

‡B.M. and S.C.contributed equally to this work.

Notes

The authors declare no competing financial interest.

■ ACKNOWLEDGMENTS

This research was funded by DST/TMD/HFC/2K18/90 and SERB EMR-080063. S.C. deeply acknowledges the IACS Integrated Ph.D. program. Z.G. and A.M. acknowledge the financial support of this research by the Israel Science Foundation.

■ REFERENCES

(1) Cox, N.; Pantazis, D. A.; Lubitz, W. Current Understanding of the Mechanism of Water Oxidation in Photosystem II and Its Relation to XFEL Data. *Annu. Rev. Biochem.* **2020**, *89* (1), 795–820.

(2) Cox, N.; Pantazis, D. A.; Neese, F.; Lubitz, W. Biological Water Oxidation. *Acc. Chem. Res.* **2013**, *46* (7), 1588–1596.

(3) Sala, X.; Maji, S.; Bofill, R.; García-Antón, J.; Escriche, L.; Llobet, A. Molecular Water Oxidation Mechanisms Followed by Transition Metals: State of the Art. *Acc. Chem. Res.* **2014**, *47* (2), 504–516.

(4) Duan, L.; Wang, L.; Li, F.; Li, F.; Sun, L. Highly Efficient Bioinspired Molecular Ru Water Oxidation Catalysts with Negatively Charged Backbone Ligands. *Acc. Chem. Res.* **2015**, *48* (7), 2084–2096.

(5) Hammarström, L. Accumulative Charge Separation for Solar Fuels Production: Coupling Light-Induced Single Electron Transfer to Multielectron Catalysis. *Acc. Chem. Res.* **2015**, *48* (3), 840–850.

(6) Young, K. J.; Brennan, B. J.; Tagore, R.; Brudvig, G. W. Photosynthetic Water Oxidation: Insights from Manganese Model Chemistry. *Acc. Chem. Res.* **2015**, *48* (3), 567–574.

https://dx.doi.org/10.1021/jacs.0c08654
J. Am. Chem. Soc. XXXX, XXX, XXX–XXX

(7) Brudvig, G. W.; Thorp, H. H.; Crabtree, R. H. Probing the mechanism of water oxidation in photosystem II. *Acc. Chem. Res.* **1991**, *24* (10), 311−316.
(8) Concepcion, J. J.; Jurss, J. W.; Brennaman, M. K.; Hoertz, P. G.; Patrocinio, A. O. T.; Murakami Iha, N. Y.; Templeton, J. L.; Meyer, T. J. Making Oxygen with Ruthenium Complexes. *Acc. Chem. Res.* **2009**, *42* (12), 1954−1965.
(9) Garrido-Barros, P.; Matheu, R.; Gimbert-Suriñach, C.; Llobet, A. Electronic, mechanistic, and structural factors that influence the performance of molecular water oxidation catalysts anchored on electrode surfaces. *Current Opinion in Electrochemistry* **2019**, *15*, 140−147.
(10) Matheu, R.; Garrido-Barros, P.; Gil-Sepulcre, M.; Ertem, M. Z.; Sala, X.; Gimbert-Suriñach, C.; Llobet, A. The development of molecular water oxidation catalysts. *Nat. Rev. Chem.* **2019**, *3* (5), 331−341.
(11) Hunter, B. M.; Gray, H. B.; Müller, A. M. Earth-Abundant Heterogeneous Water Oxidation Catalysts. *Chem. Rev.* **2016**, *116* (22), 14120−14136.
(12) Liu, J.; Zou, Y.; Jin, B.; Zhang, K.; Park, J. H. Hydrogen Peroxide Production from Solar Water Oxidation. *ACS Energy Lett.* **2019**, *4* (12), 3018−3027.
(13) Blakemore, J. D.; Crabtree, R. H.; Brudvig, G. W. Molecular Catalysts for Water Oxidation. *Chem. Rev.* **2015**, *115* (23), 12974−13005.
(14) Pantazis, D. A. Missing Pieces in the Puzzle of Biological Water Oxidation. *ACS Catal.* **2018**, *8* (10), 9477−9507.
(15) Kärkäs, M. D.; Verho, O.; Johnston, E. V.; Åkermark, B. Artificial Photosynthesis: Molecular Systems for Catalytic Water Oxidation. *Chem. Rev.* **2014**, *114* (24), 11863−12001.
(16) Viswanathan, V.; Hansen, H. A.; Nørskov, J. K. Selective Electrochemical Generation of Hydrogen Peroxide from Water Oxidation. *J. Phys. Chem. Lett.* **2015**, *6* (21), 4224−4228.
(17) Shi, X.; Siahrostami, S.; Li, G.-L.; Zhang, Y.; Chakthranont, P.; Studt, F.; Jaramillo, T. F.; Zheng, X.; Nørskov, J. K. Understanding activity trends in electrochemical water oxidation to form hydrogen peroxide. *Nat. Commun.* **2017**, *8* (1), 701.
(18) Liu, Y.; Han, Y.; Zhang, Z.; Zhang, W.; Lai, W.; Wang, Y.; Cao, R. Low overpotential water oxidation at neutral pH catalyzed by a copper(ii) porphyrin. *Chem. Sci.* **2019**, *10* (9), 2613−2622.
(19) Kelly, S. R.; Shi, X.; Back, S.; Vallez, L.; Park, S. Y.; Siahrostami, S.; Zheng, X.; Nørskov, J. K. ZnO As an Active and Selective Catalyst for Electrochemical Water Oxidation to Hydrogen Peroxide. *ACS Catal.* **2019**, *9* (5), 4593−4599.
(20) Li, L.; Hu, Z.; Yu, J. C. On-Demand Synthesis of H_2O_2 by Water Oxidation for Sustainable Resource Production and Organic Pollutant Degradation. *Angew. Chem., Int. Ed.* **2020**, *59*, 20538−20544.
(21) Xia, C.; Back, S.; Ringe, S.; Jiang, K.; Chen, F.; Sun, X.; Siahrostami, S.; Chan, K.; Wang, H. Confined local oxygen gas promotes electrochemical water oxidation to hydrogen peroxide. *Nat. Catal.* **2020**, *3* (2), 125−134.
(22) Ponce de León, C. In situ anodic generation of hydrogen peroxide. *Nat. Catal.* **2020**, *3* (2), 96−97.
(23) Schöfberger, W.; Faschinger, F.; Chattopadhyay, S.; Bhakta, S.; Mondal, B.; Elemans, J. A. A. W.; Müllegger, S.; Tebi, S.; Koch, R.; Klappenberger, F.; Paszkiewicz, M.; Barth, J. V.; Rauls, E.; Aldahhak, H.; Schmidt, W. G.; Dey, A. A Bifunctional Electrocatalyst for Oxygen Evolution and Oxygen Reduction Reactions in Water. *Angew. Chem., Int. Ed.* **2016**, *55* (7), 2350−2355.
(24) Sheehan, S. W.; Thomsen, J. M.; Hintermair, U.; Crabtree, R. H.; Brudvig, G. W.; Schmuttenmaer, C. A. A molecular catalyst for water oxidation that binds to metal oxide surfaces. *Nat. Commun.* **2015**, *6*, 6469.
(25) Retegan, M.; Krewald, V.; Mamedov, F.; Neese, F.; Lubitz, W.; Cox, N.; Pantazis, D. A. A five-coordinate Mn(IV) intermediate in biological water oxidation: spectroscopic signature and a pivot mechanism for water binding. *Chem. Sci.* **2016**, *7* (1), 72−84.
(26) Okamura, M.; Kondo, M.; Kuga, R.; Kurashige, Y.; Yanai, T.; Hayami, S.; Praneeth, V. K. K.; Yoshida, M.; Yoneda, K.; Kawata, S.; Masaoka, S. A pentanuclear iron catalyst designed for water oxidation. *Nature* **2016**, *530* (7591), 465−468.
(27) Lapides, A. M.; Sherman, B. D.; Brennaman, M. K.; Dares, C. J.; Skinner, K. R.; Templeton, J. L.; Meyer, T. J. Synthesis, characterization, and water oxidation by a molecular chromophore-catalyst assembly prepared by atomic layer deposition. The "mummy" strategy. *Chem. Sci.* **2015**, *6* (11), 6398−6406.
(28) Codolà, Z.; Gómez, L.; Kleespies, S. T.; Que, L., Jr; Costas, M.; Lloret-Fillol, J. Evidence for an oxygen evolving iron-oxo-cerium intermediate in iron-catalysed water oxidation. *Nat. Commun.* **2015**, *6*, 5865.
(29) Barnett, S. M.; Goldberg, K. I.; Mayer, J. M. A soluble copper-bipyridine water-oxidation electrocatalyst. *Nat. Chem.* **2012**, *4* (6), 498−502.
(30) Chen, Z.; Meyer, T. J. Copper(II) Catalysis of Water Oxidation. *Angew. Chem., Int. Ed.* **2013**, *52* (2), 700−703.
(31) Nguyen, A. I.; Ziegler, M. S.; Oña-Burgos, P.; Sturzbecher-Hohne, M.; Kim, W.; Bellone, D. E.; Tilley, T. D. Mechanistic Investigations of Water Oxidation by a Molecular Cobalt Oxide Analogue: Evidence for a Highly Oxidized Intermediate and Exclusive Terminal Oxo Participation. *J. Am. Chem. Soc.* **2015**, *137* (40), 12865−12872.
(32) Wang, D.; Groves, J. T. Efficient water oxidation catalyzed by homogeneous cationic cobalt porphyrins with critical roles for the buffer base. *Proc. Natl. Acad. Sci. U. S. A.* **2013**, *110* (39), 15579−15584.
(33) Nakazono, T.; Parent, A. R.; Sakai, K. Cobalt porphyrins as homogeneous catalysts for water oxidation. *Chem. Commun.* **2013**, *49* (56), 6325−6327.
(34) Brunschwig, B. S.; Chou, M. H.; Creutz, C.; Ghosh, P.; Sutin, N. Mechanisms of water oxidation to oxygen: cobalt(IV) as an intermediate in the aquocobalt(II)-catalyzed reaction. *J. Am. Chem. Soc.* **1983**, *105* (14), 4832−4833.
(35) Dey, S.; Mondal, B.; Dey, A. An acetate bound cobalt oxide catalyst for water oxidation: role of monovalent anions and cations in lowering overpotential. *Phys. Chem. Chem. Phys.* **2014**, *16* (24), 12221−12227.
(36) Han, A.; Jia, H.; Ma, H.; Ye, S.; Wu, H.; Lei, H.; Han, Y.; Cao, R.; Du, P. Cobalt porphyrin electrode films for electrocatalytic water oxidation. *Phys. Chem. Chem. Phys.* **2014**, *16* (23), 11224−11232.
(37) Hong, S.; Pfaff, F. F.; Kwon, E.; Wang, Y.; Seo, M.-S.; Bill, E.; Ray, K.; Nam, W. Spectroscopic Capture and Reactivity of a Low-Spin Cobalt(IV)-Oxo Complex Stabilized by Binding Redox-Inactive Metal Ions. *Angew. Chem., Int. Ed.* **2014**, *53* (39), 10403−10407.
(38) Lin, C.-Y.; Mersch, D.; Jefferson, D. A.; Reisner, E. Cobalt sulphide microtube array as cathode in photoelectrochemical water splitting with photoanodes. *Chem. Sci.* **2014**, *5* (12), 4906−4913.
(39) Deng, X.; Tüysüz, H. Cobalt-Oxide-Based Materials as Water Oxidation Catalyst: Recent Progress and Challenges. *ACS Catal.* **2014**, *4* (10), 3701−3714.
(40) Li, J.; Wan, W.; Triana, C. A.; Novotny, Z.; Osterwalder, J.; Erni, R.; Patzke, G. R. Dynamic Role of Cluster Cocatalysts on Molecular Photoanodes for Water Oxidation. *J. Am. Chem. Soc.* **2019**, *141* (32), 12839−12848.
(41) Wu, Q.; Xiao, M.; Wang, W.; Cui, C. In Situ Coordination Environment Tuning of Cobalt Sites for Efficient Water Oxidation. *ACS Catal.* **2019**, *9* (12), 11734−11742.
(42) Mohammadi, M. R.; Loos, S.; Chernev, P.; Pasquini, C.; Zaharieva, I.; González-Flores, D.; Kubella, P.; Klingan, K.; Smith, R. D. L.; Dau, H. Exploring the Limits of Self-Repair in Cobalt Oxide Films for Electrocatalytic Water Oxidation. *ACS Catal.* **2020**, *10* (14), 7990−7999.
(43) Biswas, S.; Bose, S.; Debgupta, J.; Das, P.; Biswas, A. N. Redox-active ligand assisted electrocatalytic water oxidation by a mononuclear cobalt complex. *Dalton Trans.* **2020**, *49* (21), 7155−7165.

https://dx.doi.org/10.1021/jacs.0c08654
J. Am. Chem. Soc. XXXX, XXX, XXX−XXX

(44) Hong, Y. H.; Han, J. W.; Jung, J.; Nakagawa, T.; Lee, Y.-M.; Nam, W.; Fukuzumi, S. Photocatalytic Oxygenation Reactions with a Cobalt Porphyrin Complex Using Water as an Oxygen Source and Dioxygen as an Oxidant. *J. Am. Chem. Soc.* **2019**, *141* (23), 9155−9159.
(45) Ullman, A. M.; Brodsky, C. N.; Li, N.; Zheng, S.-L.; Nocera, D. G. Probing Edge Site Reactivity of Oxidic Cobalt Water Oxidation Catalysts. *J. Am. Chem. Soc.* **2016**, *138* (12), 4229−4236.
(46) Costentin, C.; Nocera, D. G. Self-healing catalysis in water. *Proc. Natl. Acad. Sci. U. S. A.* **2017**, *114* (51), 13380.
(47) Kanan, M. W.; Surendranath, Y.; Nocera, D. G. Cobalt-phosphate oxygen-evolving compound. *Chem. Soc. Rev.* **2009**, *38* (1), 109−114.
(48) Young, E. R.; Costi, R.; Paydavosi, S.; Nocera, D. G.; Bulović, V. Photo-assisted water oxidation with cobalt-based catalyst formed from thin-film cobalt metal on silicon photoanodes. *Energy Environ. Sci.* **2011**, *4* (6), 2058−2061.
(49) Risch, M.; Ringleb, F.; Kohlhoff, M.; Bogdanoff, P.; Chernev, P.; Zaharieva, I.; Dau, H. Water oxidation by amorphous cobalt-based oxides: in situ tracking of redox transitions and mode of catalysis. *Energy Environ. Sci.* **2015**, *8* (2), 661−674.
(50) Golubkov, G.; Bendix, J.; Gray, H. B.; Mahammed, A.; Goldberg, I.; DiBilio, A. J.; Gross, Z. High-Valent Manganese Corroles and the First Perhalogenated Metallocorrole Catalyst. *Angew. Chem., Int. Ed.* **2001**, *40* (11), 2132−2134.
(51) Gross, Z. High-valent corrole metal complexes. *JBIC, J. Biol. Inorg. Chem.* **2001**, *6* (7), 733−738.
(52) Meier-Callahan, A. E.; Di Bilio, A. J.; Simkhovich, L.; Mahammed, A.; Goldberg, I.; Gray, H. B.; Gross, Z. Chromium Corroles in Four Oxidation States. *Inorg. Chem.* **2001**, *40* (26), 6788−6793.
(53) Simkhovich, L.; Gross, Z. Iron(IV) corroles are potent catalysts for aziridination of olefins by Chloramine-T. *Tetrahedron Lett.* **2001**, *42* (45), 8089−8092.
(54) Steene, E.; Wondimagegn, T.; Ghosh, A. Electrochemical and Electronic Absorption Spectroscopic Studies of Substituent Effects in Iron(IV) and Manganese(IV) Corroles. Do the Compounds Feature High-Valent Metal Centers or Noninnocent Corrole Ligands? Implications for Peroxidase Compound I and II Intermediates. *J. Phys. Chem. B* **2001**, *105* (46), 11406−11413.
(55) Ghosh, A.; Steene, E. High-valent transition metal centers versus noninnocent ligands in metallocorroles: insights from electrochemistry and implications for high-valent heme protein intermediates. *J. Inorg. Biochem.* **2002**, *91* (3), 423−436.
(56) Grodkowski, J.; Neta, P.; Fujita, E.; Mahammed, A.; Simkhovich, L.; Gross, Z. Reduction of Cobalt and Iron Corroles and Catalyzed Reduction of CO_2. *J. Phys. Chem. A* **2002**, *106* (18), 4772−4778.
(57) Golubkov, G.; Gross, Z. Chromium(V) and Chromium(VI) Nitrido Complexes of Tris(pentafluorophenyl)corrole. *Angew. Chem., Int. Ed.* **2003**, *42* (37), 4507−4510.
(58) Dogutan, D. K.; Stoian, S. A.; McGuire, R.; Schwalbe, M.; Teets, T. S.; Nocera, D. G. Hangman Corroles: Efficient Synthesis and Oxygen Reaction Chemistry. *J. Am. Chem. Soc.* **2011**, *133* (1), 131−140.
(59) Lei, H.; Han, A.; Li, F.; Zhang, M.; Han, Y.; Du, P.; Lai, W.; Cao, R. Electrochemical, spectroscopic and theoretical studies of a simple bifunctional cobalt corrole catalyst for oxygen evolution and hydrogen production. *Phys. Chem. Chem. Phys.* **2014**, *16* (5), 1883−1893.
(60) Mondal, B.; Sengupta, K.; Rana, A.; Mahammed, A.; Botoshansky, M.; Dey, S. G.; Gross, Z.; Dey, A. Cobalt Corrole Catalyst for Efficient Hydrogen Evolution Reaction from H2O under Ambient Conditions: Reactivity, Spectroscopy, and Density Functional Theory Calculations. *Inorg. Chem.* **2013**, *52* (6), 3381−3387.
(61) Mahammed, A.; Mondal, B.; Rana, A.; Dey, A.; Gross, Z. The cobalt corrole catalyzed hydrogen evolution reaction: surprising electronic effects and characterization of key reaction intermediates. *Chem. Commun.* **2014**, *50* (21), 2725−2727.
(62) Wang, Z.; Lei, H.; Cao, R.; Zhang, M. Cobalt Corrole on Carbon Nanotube as a Synergistic Catalyst for Oxygen Reduction Reaction in Acid Media. *Electrochim. Acta* **2015**, *171*, 81−88.
(63) Levy, N.; Mahammed, A.; Kosa, M.; Major, D. T.; Gross, Z.; Elbaz, L. Metallocorroles as Nonprecious-Metal Catalysts for Oxygen Reduction. *Angew. Chem., Int. Ed.* **2015**, *54* (47), 14080−14084.
(64) Schechter, A.; Stanevsky, M.; Mahammed, A.; Gross, Z. Four-Electron Oxygen Reduction by Brominated Cobalt Corrole. *Inorg. Chem.* **2012**, *51* (1), 22−24.
(65) Mahammed, A.; Gross, Z. Metallocorroles as Photocatalysts for Driving Endergonic Reactions, Exemplified by Bromide to Bromine Conversion. *Angew. Chem., Int. Ed.* **2015**, *54* (42), 12370−12373.
(66) Zipp, C. F.; Michael, J. P.; Fernandes, M. A.; Mathura, S.; Perry, C. B.; Navizet, I.; Govender, P. P.; Marques, H. M. The Synthesis of a Corrole Analogue of Aquacobalamin (Vitamin B_{12a}) and Its Ligand Substitution Reactions. *Inorg. Chem.* **2014**, *53* (9), 4418−4429.
(67) Albrett, A. M.; Conradie, J.; Boyd, P. D. W.; Clark, G. R.; Ghosh, A.; Brothers, P. J. Corrole as a Binucleating Ligand: Preparation, Molecular Structure and Density Functional Theory Study of Diboron Corroles. *J. Am. Chem. Soc.* **2008**, *130* (10), 2888−2889.
(68) Dogutan, D. K.; McGuire, R.; Nocera, D. G. Electocatalytic Water Oxidation by Cobalt(III) Hangman Î²-Octafluoro Corroles. *J. Am. Chem. Soc.* **2011**, *133* (24), 9178−9180.
(69) Mahammed, A.; Tumanskii, B.; Gross, Z. Effect of bromination on the electrochemistry, frontier orbitals, and spectroscopy of metallocorroles. *J. Porphyrins Phthalocyanines* **2011**, *15* (11n12), 1275−1286.
(70) Mahammed, A.; Gray, H. B.; Meier-Callahan, A. E.; Gross, Z. Aerobic Oxidations Catalyzed by Chromium Corroles. *J. Am. Chem. Soc.* **2003**, *125* (5), 1162−1163.
(71) Ertem, M. Z.; Cramer, C. J. Quantum chemical characterization of the mechanism of a supported cobalt-based water oxidation catalyst. *Dalton Trans.* **2012**, *41* (39), 12213−12219.
(72) Lai, W.; Cao, R.; Dong, G.; Shaik, S.; Yao, J.; Chen, H. Why Is Cobalt the Best Transition Metal in Transition-Metal Hangman Corroles for O-O Bond Formation during Water Oxidation? *J. Phys. Chem. Lett.* **2012**, *3* (17), 2315−2319.
(73) Liu, F.; Concepcion, J. J.; Jurss, J. W.; Cardolaccia, T.; Templeton, J. L.; Meyer, T. J. Mechanisms of Water Oxidation from the Blue Dimer to Photosystem II. *Inorg. Chem.* **2008**, *47* (6), 1727−1752.
(74) Stull, J. A.; Stich, T. A.; Hurst, J. K.; Britt, R. D. Electron Paramagnetic Resonance Analysis of a Transient Species Formed During Water Oxidation Catalyzed by the Complex Ion $[(bpy)_2Ru(OH_2)]_2O^{4+}$. *Inorg. Chem.* **2013**, *52* (8), 4578−4586.
(75) Lutterman, D. A.; Surendranath, Y.; Nocera, D. G. A Self-Healing Oxygen-Evolving Catalyst. *J. Am. Chem. Soc.* **2009**, *131* (11), 3838−3839.
(76) Kim, H.; Park, J.; Park, I.; Jin, K.; Jerng, S. E.; Kim, S. H.; Nam, K. T.; Kang, K. Coordination tuning of cobalt phosphates towards efficient water oxidation catalyst. *Nat. Commun.* **2015**, *6*, 8253.
(77) Ahn, H. S.; Bard, A. J. Surface Interrogation of CoPi Water Oxidation Catalyst by Scanning Electrochemical Microscopy. *J. Am. Chem. Soc.* **2015**, *137* (2), 612−615.
(78) Kanan, M. W.; Yano, J.; Surendranath, Y.; Dincă, M.; Yachandra, V. K.; Nocera, D. G. Structure and Valency of a Cobalt-Phosphate Water Oxidation Catalyst Determined by in Situ X-ray Spectroscopy. *J. Am. Chem. Soc.* **2010**, *132* (39), 13692−13701.
(79) Harley, S. J.; Mason, H. E.; McAlpin, J. G.; Britt, R. D.; Casey, W. H. A 31P NMR Investigation of the CoPi Water-Oxidation Catalyst. *Chem. - Eur. J.* **2012**, *18* (34), 10476−10479.
(80) Moysiadou, A.; Lee, S.; Hsu, C.-S.; Chen, H. M.; Hu, X. Mechanism of Oxygen Evolution Catalyzed by Cobalt Oxyhydroxide: Cobalt Superoxide Species as a Key Intermediate and Dioxygen Release as a Rate-Determining Step. *J. Am. Chem. Soc.* **2020**, *142*, 11901−11914.
(81) Suen, N.-T.; Hung, S.-F.; Quan, Q.; Zhang, N.; Xu, Y.-J.; Chen, H. M. Electrocatalysis for the oxygen evolution reaction: recent

https://dx.doi.org/10.1021/jacs.0c08654
J. Am. Chem. Soc. XXXX, XXX, XXX−XXX

development and future perspectives. *Chem. Soc. Rev.* **2017**, *46* (2), 337−365.
(82) Pasquini, C.; Zaharieva, I.; González-Flores, D.; Chernev, P.; Mohammadi, M. R.; Guidoni, L.; Smith, R. D. L.; Dau, H. H/D Isotope Effects Reveal Factors Controlling Catalytic Activity in Co-Based Oxides for Water Oxidation. *J. Am. Chem. Soc.* **2019**, *141* (7), 2938−2948.
(83) Surendranath, Y.; Kanan, M. W.; Nocera, D. G. Mechanistic Studies of the Oxygen Evolution Reaction by a Cobalt-Phosphate Catalyst at Neutral pH. *J. Am. Chem. Soc.* **2010**, *132* (46), 16501−16509.
(84) Gerken, J. B.; McAlpin, J. G.; Chen, J. Y. C.; Rigsby, M. L.; Casey, W. H.; Britt, R. D.; Stahl, S. S. Electrochemical Water Oxidation with Cobalt-Based Electrocatalysts from pH 0−14: The Thermodynamic Basis for Catalyst Structure, Stability, and Activity. *J. Am. Chem. Soc.* **2011**, *133* (36), 14431−14442.
(85) Bhunia, S.; Rana, A.; Roy, P.; Martin, D. J.; Pegis, M. L.; Roy, B.; Dey, A. Rational Design of Mononuclear Iron Porphyrins for Facile and Selective $4e^-/4H^+$ O_2 Reduction: Activation of O-O Bond by 2nd Sphere Hydrogen Bonding. *J. Am. Chem. Soc.* **2018**, *140* (30), 9444−9457.
(86) Dey, S.; Mondal, B.; Chatterjee, S.; Rana, A.; Amanullah, S.; Dey, A. Molecular electrocatalysts for the oxygen reduction reaction. *Nat. Rev. Chem.* **2017**, *1* (12), 0098.
(87) Chatterjee, S.; Sengupta, K.; Mondal, B.; Dey, S.; Dey, A. Factors Determining the Rate and Selectivity of $4e^-/4H^+$ Electrocatalytic Reduction of Dioxygen by Iron Porphyrin Complexes. *Acc. Chem. Res.* **2017**, *50* (7), 1744−1753.
(88) Ghatak, A.; Bhakta, S.; Bhunia, S.; Dey, A. Influence of the distal guanidine group on the rate and selectivity of O2 reduction by iron porphyrin. *Chem. Sci.* **2019**, *10* (42), 9692−9698.
(89) Vereshchuk, N.; Matheu, R.; Benet-Buchholz, J.; Pipelier, M.; Lebreton, J.; Dubreuil, D.; Tessier, A.; Gimbert-Suriñach, C.; Ertem, M. Z.; Llobet, A. Second Coordination Sphere Effects in an Evolved Ru Complex Based on Highly Adaptable Ligand Results in Rapid Water Oxidation Catalysis. *J. Am. Chem. Soc.* **2020**, *142* (11), 5068−5077.
(90) Sinha, W.; Mizrahi, A.; Mahammed, A.; Tumanskii, B.; Gross, Z. Reactive Intermediates Involved in Cobalt Corrole Catalyzed Water Oxidation (and Oxygen Reduction). *Inorg. Chem.* **2018**, *57* (1), 478−485.
(91) Stracke, J. J.; Finke, R. G. Electrocatalytic Water Oxidation Beginning with the Cobalt Polyoxometalate $[Co_4(H_2O)_2(PW_9O_{34})_2]^{10-}$: Identification of Heterogeneous CoOx as the Dominant Catalyst. *J. Am. Chem. Soc.* **2011**, *133* (38), 14872−14875.
(92) Crabtree, R. H. Resolving Heterogeneity Problems and Impurity Artifacts in Operationally Homogeneous Transition Metal Catalysts. *Chem. Rev.* **2012**, *112* (3), 1536−1554.
(93) Das, D.; Pattanayak, S.; Singh, K. K.; Garai, B.; Sen Gupta, S. Electrocatalytic water oxidation by a molecular cobalt complex through a high valent cobalt oxo intermediate. *Chem. Commun.* **2016**, *52* (79), 11787−11790.
(94) Ramdhanie, B.; Telser, J.; Caneschi, A.; Zakharov, L. N.; Rheingold, A. L.; Goldberg, D. P. An Example of O_2 Binding in a Cobalt(II) Corrole System and High-Valent Cobalt-Cyano and Cobalt-Alkynyl Complexes. *J. Am. Chem. Soc.* **2004**, *126* (8), 2515−2525.
(95) Mittra, K.; Mondal, B.; Mahammed, A.; Gross, Z.; Dey, A. Dioxygen bound cobalt corroles. *Chem. Commun.* **2017**, *53* (5), 877−880.
(96) Gao, Y.; Åkermark, T.; Liu, J.; Sun, L.; Åkermark, B. Nucleophilic Attack of Hydroxide on a Mn^V Oxo Complex: A Model of the O-O Bond Formation in the Oxygen Evolving Complex of Photosystem II. *J. Am. Chem. Soc.* **2009**, *131* (25), 8726−8727.
(97) Zhang, M.; de Respinis, M.; Frei, H. Time-resolved observations of water oxidation intermediates on a cobalt oxide nanoparticle catalyst. *Nat. Chem.* **2014**, *6* (4), 362−367.
(98) Brezny, A. C.; Johnson, S. I.; Raugei, S.; Mayer, J. M. Selectivity-Determining Steps in O_2 Reduction Catalyzed by Iron-(tetramesitylporphyrin). *J. Am. Chem. Soc.* **2020**, *142* (9), 4108−4113.
(99) Frisch, M. J.; Trucks, G. W.; Schlegel, H. B.; Scuseria, G. E.; Robb, M. A.; Cheeseman, J. R.; Montgomery, J. A., Jr; Vreven, T.; Kudin, K. N.; Burant, J. C.; Millam, J. M.; Iyengar, S. S.; Tomasi, J.; Barone, V.; Mennucci, B.; Cossi, M.; Scalmani, G.; Rega, N.; Petersson, G. A.; Nakatsuji, H.; Hada, M.; Ehara, M.; Toyota, K.; Fukuda, R.; Hasegawa, J.; Ishida, M.; Nakajima, T.; Honda, Y.; Kitao, O.; Nakai, H.; Klene, M.; Li, X.; Knox, J. E.; Hratchian, H. P.; Cross, J. B.; Bakken, V.; Adamo, C.; Jaramillo, J.; Gomperts, R.; Stratmann, R. E.; Yazyev, O.; Austin, A. J.; Cammi, R.; Pomelli, C.; Ochterski, J. W.; Ayala, P. Y.; Morokuma, K.; Voth, G. A.; Salvador, P.; Dannenberg, J. J.; Zakrzewski, V. G.; Dapprich, S.; Daniels, A. D.; Strain, M. C.; Farkas, O.; Malick, D. K.; Rabuck, A. D.; Raghavachari, K.; Foresman, J. B.; Ortiz, J. V.; Cui, Q.; Baboul, A. G.; Clifford, S.; Cioslowski, J.; Stefanov, B. B.; Liu, G.; Liashenko, A.; Piskorz, P.; Komaromi, I.; Martin, R. L.; Fox, D. J.; Keith, T.; Al-Laham, M. A.; Peng, C. Y.; Nanayakkara, A.; Challacombe, M.; Gill, P. M. W.; Johnson, B.; Chen, W.; Wong, M. W.; Gonzalez, C.; Pople, J. A *Gaussian 03*, Revision C.02; Gaussian, Inc.: Wallingford, CT, 2004.
(100) Krishnan, R.; Binkley, J. S.; Seeger, R.; Pople, J. A. Self-consistent molecular orbital methods. XX. A basis set for correlated wave functions. *J. Chem. Phys.* **1980**, *72* (1), 650−654.
(101) McLean, A. D.; Chandler, G. S. Contracted Gaussian basis sets for molecular calculations. I. Second row atoms, Z = 11−18. *J. Chem. Phys.* **1980**, *72* (10), 5639−5648.

https://dx.doi.org/10.1021/jacs.0c08654
J. Am. Chem. Soc. XXXX, XXX, XXX−XXX